Applied Catalysis B: Environmental 182 (2016) 405–413

Contents lists available at ScienceDirect

Applied Catalysis B: Environmental

journal homepage: www.elsevier.com/locate/apcatb

Photocatalytic decomposition of hydrogen peroxide over nanoparticles of TiO_2 and Ni(II)-porphyrin-doped TiO_2: A relationship between activity and porphyrin anchoring mode

Ludivine Tasseroul*, Carlos A. Páez, Stéphanie D. Lambert, David Eskenazi, Benoît Heinrichs

University of Liège, Department of Chemical Engineering—Nanomaterials Catalysis and Electrochemistry, B6a, B-4000 Liège, Belgium

ARTICLE INFO

Article history:
Received 2 June 2015
Received in revised form
14 September 2015
Accepted 18 September 2015
Available online 25 September 2015

Keywords:
TiO_2 sensitization
Nickel tetra(4-carboxyphenyl)porphyrin (TCPPNi)
Porphyrin anchoring
Hydrogen peroxide photodegradation
O_2-production monitoring

ABSTRACT

The nickel tetra(4-carboxyphenyl)porphyrin (TCPPNi) was chimisorbed on Degussa P25 TiO_2 at different concentrations. Diffuse reflectance spectroscopy in the UV/vis region, Fourier transform infrared spectroscopy and thermal gravimetry combined with differential scanning calorimetry measurements allowed the determination of the TCPPNi anchoring mode. At low TCPPNi concentrations, this anchoring on Degussa P25 TiO_2 took place through all four carboxylic groups, while at higher concentrations the anchoring occurred through one or two carboxylic groups. For the first time, the effect of UV/vis light irradiation on the H_2O_2-degradation activity of TiO_2 and TCPPNi-doped TiO_2 was studied using the method of following the production of O_2 by gas pressure monitoring. The activity of seven different catalysts was related to the TCPPNi anchoring mode and the percentage of TiO_2 Degussa P25 coverage. An optimum degradation of H_2O_2 was observed for 0.0115 mol TCPPNi $\times g^{-1}$ P25. In that case, the TCPPNi was anchored through the four carboxylic groups, corresponding to a strong interaction with Degussa P25 TiO_2. Moreover, the TCPPNi did not cover the surface completely, therefore allowing the light to reach and activate the TiO_2.

1. Introduction

Since the discovery by Fujishima and Honda [1] of the photocatalytic decomposition of water on TiO_2, heterogeneous photocatalysis has been widely studied for its environmental applications. Many compounds present in effluents, such as dyes, drug metabolites and pesticides, are not biodegradable, and advanced oxidative processes represent new technologies for treating these compounds in waste water [2]. The compounds are not readily degraded by biological or chemical methods such as the activated sludge or coagulation–flocculation processes used in conventional waste water treatments [2,3]. By contrast, photo-oxidative processes can completely destroy organic pollutants such as alkanes, pesticides, dyes, *etc.* [4]. Under UV–vis light irradiation, the photocatalytic activity of TiO_2 results from the injection of electrons into the conduction band ($TiO_2(e^-_{CB})$), which leaves holes in the valence band ($TiO_2(h^+_{VB})$) [5]. These electrons and holes allow the formation of active species such as: $O_2^{\bullet -}$, $HO_2^{\bullet}$, $OH^{\bullet}$, which are involved in the degradation of pollutants [6]:

$$TiO_2 + h\nu \rightarrow TiO_2(e^-_{CB}) + TiO_2(h^+_{VB}) \quad (R1)$$

$$TiO_2(h^+_{VB}) + H_2O \rightarrow TiO_2 + H^+ + OH^{\bullet} \quad (R2)$$

$$TiO_2(h^+_{VB}) + OH^- \rightarrow TiO_2 + OH^{\bullet} \quad (R3)$$

$$TiO_2(e^-_{CB}) + O_2 \rightarrow TiO_2 + O_2^{\bullet -} \quad (R4)$$

$$O_2^{\bullet -} + H^+ \rightarrow HO_2^{\bullet} \quad (R5)$$

In addition, an important intermediate step in the photodegradation mechanism is the generation of H_2O_2 [7] following Reactions (R6) and (R7) [7–9]:

$$2e^- + 2H^+ + O_2 \leftrightarrow H_2O_2 \quad (R6)$$

$$2HO_2^{\bullet} \leftrightarrow H_2O_2 + O_2 \quad (R7)$$

H_2O_2 may also be photodecomposed to produce the active species $OH^{\bullet}$. Decomposition of H_2O_2 on TiO_2 surfaces under UV/vis light irradiation is usually investigated in order to study photodegradation mechanisms by complex methodologies such as

* Corresponding author.
E-mail address: ltasseroul@ulg.ac.be (L. Tasseroul).

http://dx.doi.org/10.1016/j.apcatb.2015.09.042
0926-3373/

electron paramagnetic resonance [10], luminol chemiluminescence probing [11], terephthalic acid fluorescence probing [11], photometric methods using *N*,*N*-diethyl-*p*-phenylenediamine [12] or iodide [13] and gas chromatography equipped with a noise-optimized pre-amplifier [14].

Moreover, the decomposition of H_2O_2 is also used to evaluate the oxidation–reduction properties of potential electrode materials such as MnO_2, $NiO–Al_2O_3$, $Ag–Al_2O_3$, *etc.* [15,16]. Main studies are focused on the enhancement of efficiency in the photocatalytic degradation of organic pollutants, or else they study the mechanisms and the kinetic behaviours of H_2O_2 in UV/vis irradiated aqueous TiO_2 suspensions [10,11,13]. In addition, in order to study the direct dissociation of H_2O_2 to produce $OH^\bullet$ under UV-irradiation [10,17], numerous electronic transfer processes from catalysts to H_2O_2 [16,18] or *vice versa* have also been proposed [18]. Several studies have shown that photo-Fenton or Fenton-like reactions with metal ions (M^{n+}, $M^{(n-1)+}$) occur through two possible electronic transfer processes: (i) if the H_2O_2 gives an electron to the metallic center (M^{n+}), then hydroperoxyl radicals ($^\bullet OOH$) are obtained (R9) [19,20] and (ii) if H_2O_2 accepts the electron from the metallic center $M^{(n-1)+}$, then hydroxyl radicals ($^\bullet OH$) are generated [19,21–24]. These reactions are similar to those observed in the photoelectronic transfer process catalyzed by TiO_2. In this case, the H_2O_2 accepts an electron from photoexcited TiO_2 (e^-_{CB}) to produce $^\bullet OH$ and OH^- (R10) [10].

$$H_2O_2 \rightarrow \tfrac{1}{2}O_2 + H_2O \quad \text{(R8)}$$

$$M^{n+} + H_2O_2 \rightarrow M^{(n-1)+} + H^+ + HO_2^\bullet \quad \text{(R9)}$$

$$M^{(n-1)+} + H_2O_2 \rightarrow M^{n+} + HO^\bullet + OH^- \quad \text{(R10)}$$

H_2O_2 decomposition can also be evaluated through a simple and inexpensive method: following the production of O_2 by gas pressure monitoring (the O_2 monitoring method) [16,20,25]. Using this method, the level of H_2O_2 decomposition (R8) is evaluated by measuring the volume of oxygen liberated at atmospheric pressure inside a gas burette. This method has been successfully used in our laboratory to study the decomposition of H_2O_2 catalyzed by manganese oxide [15]. In the present paper, the method is used to evaluate the photoactivity of TCPPNi-doped TiO_2.

One of the most widely used TiO_2 photocatalysts is commercial Degussa P25, for which the generation of oxidative species occurs when TiO_2 is exposed to UV light ($\lambda < 380$ nm). Several studies have recently been performed to extend the light absorption of TiO_2 towards the visible range. One method to do this, as used in our laboratory, is the photosensitization of a dye as porphyrins. For example, Páez et al. [26] demonstrated that the adsorption of the Ni(II) porphyrin on the surface of TiO_2 xerogels led to an improvement in the photocatalytic activity resulting in dye conversion under visible light. This porphyrin has also been introduced *in situ* into the TiO_2 matrix for *p*-nitrophenol degradation [27].

In the present study, the degradation of H_2O_2 by non-doped TiO_2 and TCPPNi-doped TiO_2 under UV/vis light is studied for the first time, using the method of O_2 production by gas pressure monitoring. The research also aims at examining the kinetic behaviour of H_2O_2 decomposition, under UV/vis light irradiation and in the dark, in relation to different TCPPNi charges.

2. Materials and method

2.1. Synthesis of catalysts

Nickel(II) tetra(4-carboxyphenyl)porphyrin (TCPPNi) was synthesized according to the method described previously [26–28]. TCPPNi FT-IR, ν (cm^{-1}): 1610 (C=C); 1560, 1515, 1490, and 1350 (P ring); 1700 (C=O); 1405, 1270 (C—O). TCPPNi ^1H NMR (CD_3OD), δ (ppm): 8.8 (*s*, 8*H*); 8.4 (*d*, 8*H*); 8.3 (*d*, 8*H*). RD-UV/vis (CH_3OH), λ (nm): TCPPNi: 405 (Soret band), 530, 582 (Q band). The TCPPNi was dissolved in methanol at six different concentrations (Table 1) and was then chimisorbed onto the commercial Degussa P25 TiO_2 according to the method described by Páez et al. [26]. TCPPNi was adsorbed overnight onto the surface of TiO_2 powder from a solution of porphyrin in methanol at room temperature and under vigorous stirring. The solid was separated by centrifugation and filtration. The amount of chimisorbed porphyrin was determined from the difference between the initial and final concentrations of TCPPNi solution measured by UV/vis absorbance at 410 nm (Table 1). Before use, catalysts were washed first in methanol and then in water for 24 h in order to remove excess TCPPNi. There was no loss of the porphyrin after successive washes as the UV/vis absorbance of the washing solutions were equal to zero. The catalysts were then dried at 100 °C overnight to remove the washing water. In order to ensure that the same treatments were applied to all the catalysts, the Degussa P25 TiO_2 without TCPPNi was also washed in methanol and then in water for 24 h before drying at 100 °C overnight. The different catalysts used were: P25, PNi/1, PNi/2, PNi/3, PNi/4, PNi/5 and PNi/6 (see Table 1).

2.2. Characterization

UV/vis spectra of methanolic solutions of TCPPNi were obtained on a Genesys 10S UV/vis (Thermo Scientific). Diffuse reflectance measurements in the UV/vis region (300–800 nm) (DR-UV/vis) were performed on a Varian Cary 500 UV/vis/NIR spectrophotometer, equipped with a Varian External DRA-2500 integrating sphere, using $BaSO_4$ as the reference. UV/vis spectra were recorded in diffuse reflectance mode (R = reflection intensity) and were transformed to the absorbance coefficient ($F(R)$) by the Kubelka–Munk function [29]:

$$F(R) = \frac{(1-R)^2}{2R} \quad (1)$$

Fourier transform infrared (FT-IR) spectra in the region of 400–4000 cm^{-1} were recorded at room temperature with a Bruker IS-88 spectrometer (resolution 4 cm^{-1}; 16 scans/spectrum). Catalyst powders were dispersed in KBr (0.6 wt.% for all samples).

The porous texture of the catalysts was investigated by nitrogen adsorption–desorption measurements. Isotherms were measured at −196 °C with a Fisons Sorptomatic 1990 after outgassing at 10^{-3} Pa for 24 h at ambient temperature. These isotherms provided the following measurements: the specific surface area obtained by the BET method, S_{BET}, the specific liquid volume adsorbed at saturation pressure of nitrogen, V_p, the specific mesopore surface area determined by the Broekhoff-de Boer method, *S*meso, and the micropore volume calculated using the Dubinin–Radushkevich method, V_m [30].

Thermal gravimetry combined with differential scanning calorimetry (TG-DSC) measurements were performed in a Setaram TG-DSC 111 thermoanalyser under air (10 mL min^{-1}). The catalysts were heated from 20 to 700 °C at 2 °C min^{-1} in a 100 μL alumina crucible. An empty crucible was used as the reference.

The catalysts were observed by fluorescence microscopy (Axioscope, Carl Zeiss MicroImaging Gmbh) in Citifluor AF87 oil.

2.3. Photocatalytic degradation of H_2O_2

The photocatalytic activity of the non-doped and TCPPNi-doped catalysts was determined *via* the degradation of H_2O_2 in aqueous solution by measuring the volume of oxygen produced per time unit at atmospheric pressure. The photoreaction was carried out using a batch reactor with external halogen lamp (300 W, 230 V) powered at 110 V (Fig. 7). The emission spectrum of the halogen lamp

Table 1
Catalysts used, the molar ratio between nickel(II) tetra(4-carboxyphenyl)-porphyrin and TiO_2 Degussa P25 and the textural properties of the catalysts.

Catalyst	Initial molar ratio (mmol TCPPNi g^{-1} P25)	Measured molar ratio (mmol TCPPNi g^{-1} P25)	S_{BET} ($m^2\ g^{-1}$) ± 5	V_p ($cm^3\ g^{-1}$) ± 0.1	S_{meso} ($m^2\ g^{-1}$) ± 5	v_m ($cm^3\ g^{-1}$) ± 0.01
P25	0	0	55	0.4	45	0.02
PNi/1	0.005	0.002	50	0.3	45	0.02
PNi/2	0.010	0.006	55	0.3	45	0.02
PNi/3	0.020	0.0115	50	0.4	45	0.02
PNi/4	0.040	0.0225	55	0.3	45	0.02
PNi/5	0.075	0.0575	50	0.3	45	0.02
PNi/6	0.125	0.0855	50	0.4	45	0.02

S_{BET}: specific surface area determined by the BET method; V_p: specific liquid volume adsorbed at the saturation pressure of nitrogen; S_{meso}: mesoporous specific surface area determined by the Broekhoff-de Boer theory; V_m: microporous volume determined by the Dubinin Radushkevitch theory

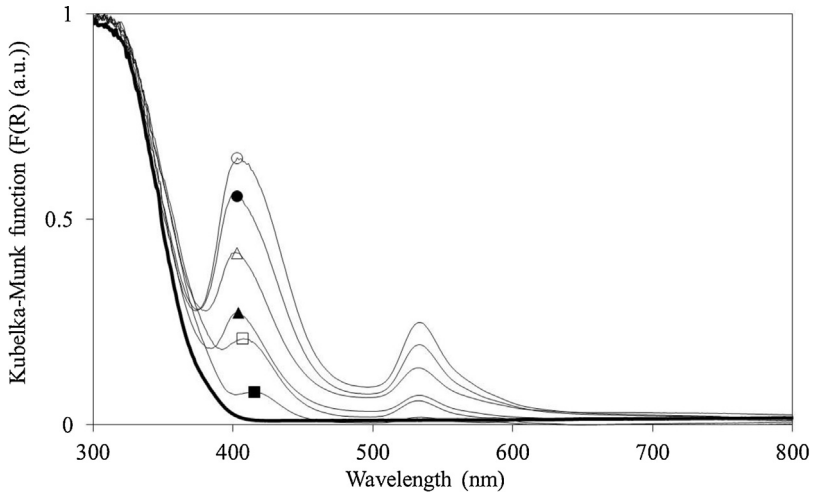

Fig. 1. DR-UV/vis spectra of catalysts P25 (▬), PNi/1 (■), PNi/2 (□), PNi/3 (▲), PNi/4 (Δ), PNi/5 (●) and PNi/6 (○).

(300 W, 230 V) was measured with a Mini-Spectrometer (Hamamatsu Photonics). This apparatus was previously described by Páez et al. [15]. A typical experiment in the present study took place as follows: (i) a known charge of catalyst was suspended in deionised water (5 mL) in the reactor and was exposed to ultra-sound for 30 min; (ii) the reactor was closed with a septum port and put back in place in the bath at 20 °C and the vigorous stirring was switched on (the pressure in the reactor at the beginning of the reaction was equal to the atmospheric pressure), (iii) 13 mL of H_2O_2 solution (30%, Merck) were injected into the catalyst suspension (5 mL) *via* the septum port; (iv) the lamp was turned on for the trials under UV/vis light radiation; (v) finally, the change in H_2O_2 concentration during photocatalytic run was determined from Eq. (2).

$$C = C_0 - 2 \times \frac{PV_g}{RTV_L} \quad (2)$$

where C is the concentration of H_2O_2 at time t (mol L^{-1}), C_0 the initial concentration of H_2O_2 (7.07 mol L^{-1}), P the atmospheric pressure (≅101.3 kPa), R is the gas constant (8.314 L kPa mol^{-1} K^{-1}), V_L the total volume of solution (0.018 L), T is the room temperature (298 K) and V_g corresponds to the integrated volume of gas liberated at time t (L) at atmospheric pressure measured by the devices mentioned. The experiment was performed with Degussa P25 TiO_2 and TCPPNi-doped Degussa P25 TiO_2 (1 g L^{-1}).

3. Results

Table 1 shows the specific surface area, S_{BET}, the specific liquid volume adsorbed at saturation pressure of nitrogen, V_p, the specific mesopore surface area, S_{meso} and the micropore volume, V_m. Initial S_{BET}, V_p, S_{meso} and V_m values were found to be low and to be the same, within experimental error, for all catalysts. Furthermore,

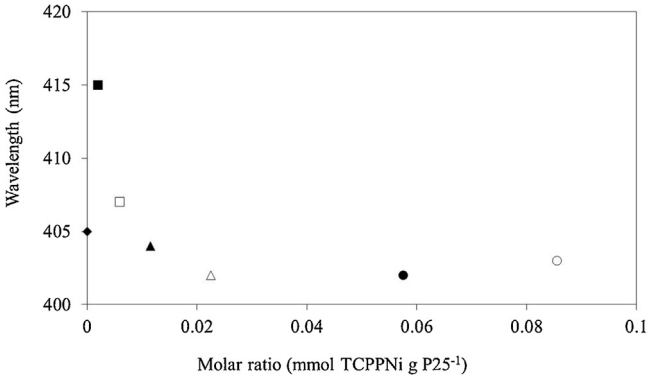

Fig. 2. Position of the absorption peak maximum observed by DR-UV/vis of catalysts PNi/1 (■), PNi/2 (□), PNi/3 (▲), PNi/4 (Δ), PNi/5 (●) and PNi/6 (○) and TCPPNi (♦).

S_{meso} (45 $cm^3\ g^{-1}$), defined as the surface developed by pores with a size ranging from 2 to 7.5 nm according to the Broekhoff-de Boer theory, were found to be the same, within experimental error, as the S_{BET} for all catalysts.

The DR-UV/vis spectra (Fig. 1) obtained in the present study indicate a maximal absorption band below 310 nm. For catalysts PNi/1 to PNi/6, absorption peaks were also observed in the visible wavelengths. These peaks correspond respectively to the Soret and the Q bands of TCPPNi. The peak intensity increased (Fig. 1) and the maximum absorption peak shifted progressively from 415 to 402 nm (Fig. 2) with the increase in TCPPNi concentration.

The FT-IR spectra obtained for all the catalysts showed some vibrations at 3300 cm^{-1} and between 1200 and 1800 cm^{-1}, which correspond to the vibration of the —OH groups and H_2O molecules

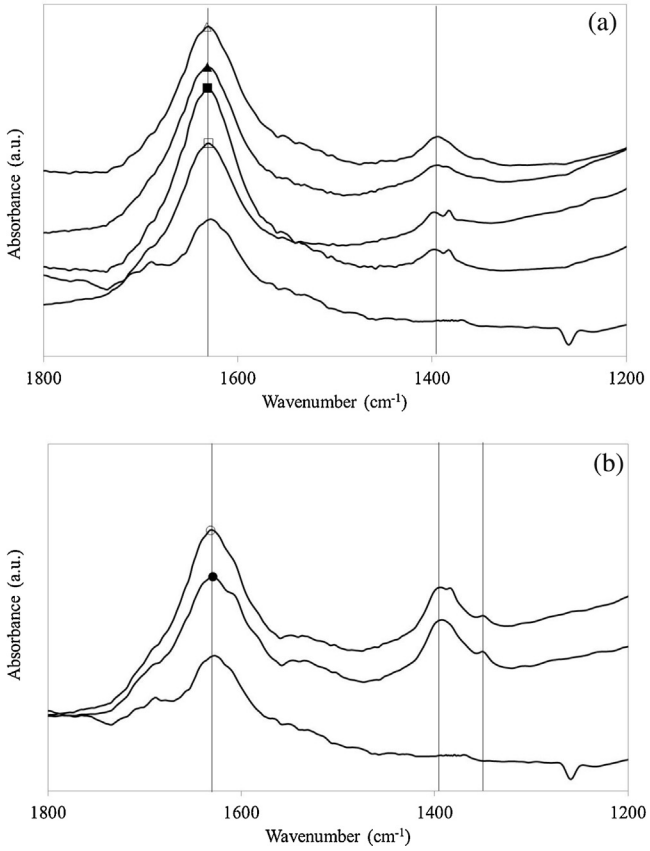

Fig. 3. FTIR spectra between 1200 and 1800 cm^{-1} of catalysts (a) P25 (—), PNi/1 (■), PNi/2 (□), PNi/3 (▲), PNi/4 (△) and (b) P25 (—), PNi/5 (●) and PNi/6 (○).

adsorbed on the TiO_2 surface. However, vibrations between 1200 and 1800 cm^{-1} presented some differences between catalysts (Fig. 3a and b). For all catalysts, the Degussa P25 TiO_2 and the TCPPNi-doped catalysts, vibrations were observed at 1630 cm^{-1}, with a higher intensity for the TCPPNi-doped catalysts than for Degussa P25 TiO_2 (Fig. 3a). Additional vibrations were observed in all the TCPPNi-doped catalysts at 1400 cm^{-1}. Finally, an additional vibration was observed at 1350 cm^{-1} for catalysts PNi/5 and PNi/6 (Fig. 3b) and the intensity of this peak increased with porphyrin concentration (Fig. 3b).

TG analyses of all the catalysts are presented in Fig. 4. The catalyst Degussa P25 TiO_2 presented almost no loss of weight and no endo- or exothermic peak between 20 and 700 °C. When the TCPPNi was chimisorbed onto P25, one loss of weight associated with one broad exothermic peak for all the catalysts was observed. The loss of weight increased and the exothermic peak temperature decreased from 430 to 350 °C with the increase in porphyrin concentration.

The fluorescence microscopy pictures of catalysts P25, PNi/3 and PNi/5 are presented in Fig. 5. Particles were observed to be blue for P25, pink to purple for PNi/3 and red for PNi/5.

The TCPPNi was found to be linked to the TiO_2 surface through a minimum one and a maximum of four carboxyl groups. The area occupied by the TCPPNi on the TiO_2 surface depended on the number of carboxyl groups involved in the linkage. In an edgewise stacking geometry, a molecule of TCPPNi was linked to the TiO_2 through two carboxyl groups and was found to occupy an area of about 0.6 nm^2 (Fig. 6a), while in a flat geometry, a molecule of TCPPNi was linked to the TiO_2 surface through 4 carboxyl groups and occupied an area of about 2.3 nm^2 (Fig. 6b). These results enabled us to calculate the percentage of TiO_2 surface area covered by TCPPNi for both types of geometry, *i.e.*, flat or edgewise stacking

Table 2
Percentage of TiO_2 surface area covered by TCPPNi according the geometry of TCPPNi

Catalyst	% of TiO_2 surface area covered by TCPPNi according to the geometry of TCPPNi	
	Flat	Edgewise stacking
P25	0	0
PNi/1	5	1
PNi/2	15	4
PNi/3	29	7.5
PNi/4	57	14.5
PNi/5	145	38
PNi/6	215	56

(Table 2). In the case of a flat geometry, more than the total surface area of P25 was found to be covered for catalysts PNi/5 (145%) and PNi/6 (215%). In the case of an edgewise stacking geometry, the TCPPNi was found not to cover the entire Degussa P25 TiO_2 surface area and to cover only half of the surface area of P25 at the highest TCPPNi concentration, *i.e.*, PNi/6.

The study of the photocatalytic degradation of H_2O_2 was initially focused on the validation of the O_2-pressure monitoring method, in the absence of a catalyst. According to the mechanism of the H_2O_2/UV oxidation process proposed by Crittenden et al. [31], the photolysis of hydrogen peroxide under UV-light follows a series of radical chain reactions. The global reaction is initiated with the photoproduction of $OH^\bullet$ and is terminated with the formation of H_2O_2 and molecular oxygen (O_2).

The overall quantum yield (Φ_T) of H_2O_2 in this reaction chain is unity (=1) at the monochromatic UV-light with $\lambda = 254$ nm. According to the Beer–Lambert law and to the definition of overall quantum yield [31], the general photolysis rate of a pure H_2O_2 solu-

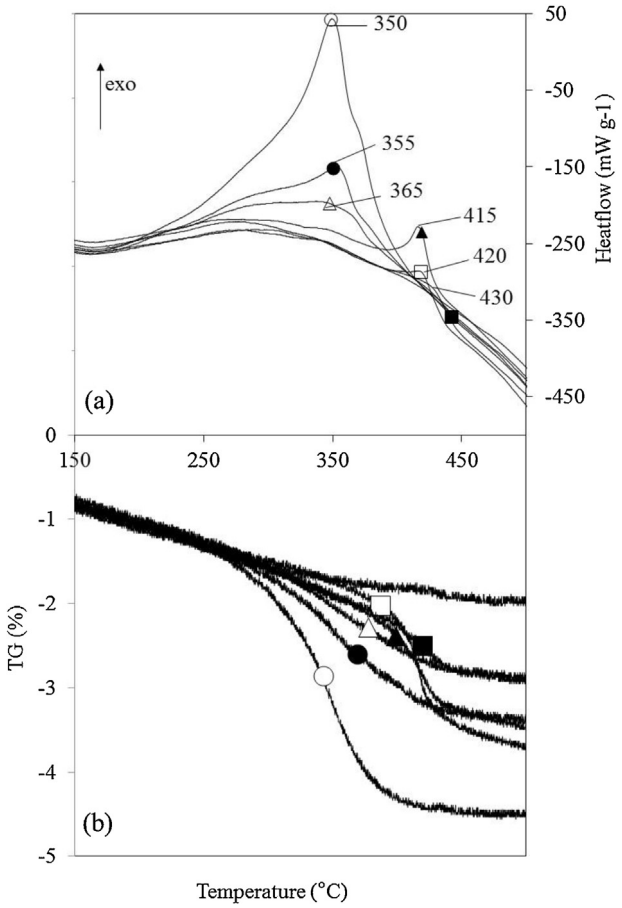

Fig. 4. TG-DSC of catalysts P25 (—), PNi/1 (■), PNi/2 (□), PNi/3 (▲), PNi/4 (△), PNi/5 (●) and PNi/6 (○).

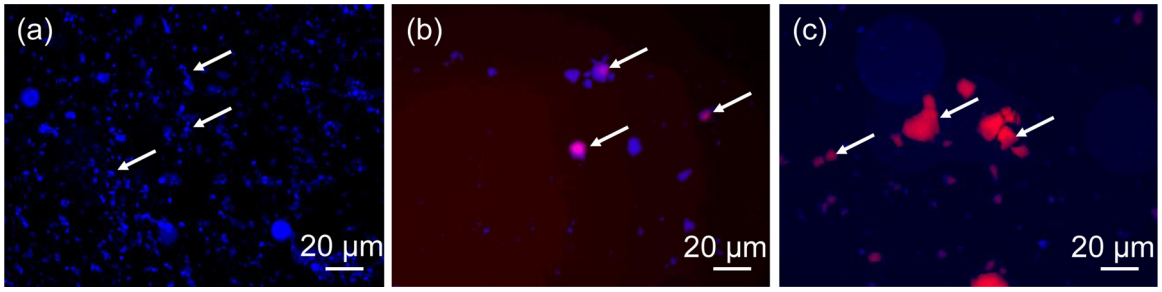

Fig. 5. Fluorescence microscopy pictures of catalysts P25 (a), PNi/3 (b) and PNi/5 (c). White arrows indicate catalyst particles. (For interpretation of the references to color in the text, the reader is referred to the web version of this article.)

tion (without: catalyst, target organic pollutants or other species) can be expressed as follows:

$$r_{H_2O_2} = -\Phi_T I_0(1 - e^{-D}) \quad (3)$$

$$D = 2.303\epsilon G b C_0, \quad (4)$$

where Φ_T is the overall quantum yield of hydrogen peroxide, I_0 is the incident UV-light intensity, ϵ is the molar extinction coefficient of H_2O_2 at I_0, b is the optical path length of the system, C_0 is the initial concentration of H_2O_2 and i is the optical density of the system. When the amount of initial concentration of H_2O_2 (C_0) is very small or very large, the expression of the general photolysis rate (Eq. (3)) can be simplified in two ways:

i) If C_0 is small, then H_2O_2-photodegradation follows a first-order kinetic (Eqs. (5) and (6)).

$$r_{H_2O_2} = -\Phi_T I_0(1 - e^{-D}) \approx -\Phi_T I_0 D \quad (5)$$

$$r_{H_2O_2} = -2.303\epsilon G b \Phi_T I_0 C_0 \quad (6)$$

- If C_0 is large, then H_2O_2-photodegradation follows a zero-order kinetic (Eq. (7)), which means that the general H_2O_2-photolysis rate ($r_{H_2O_2}$) is a linear function of the incident UV-light intensity at wavelength λ.

$$r_{H_2O_2} = -\Phi_T I_0(1 - e^{-D}) \approx -\Phi_T I_0 \quad (7)$$

In this study, the amount of initial concentration of H_2O_2 (C_0) used was very large (7.02 mol L^{-1} ≈ 22% w/w). Consequently the effect of incident UV-part of the light intensity (I_0) on the H_2O_2-photodegradation kinetic was studied. Fig. 7 shows the normalized emission spectrum of the polychromatic light source (halogen lamp powered at 110 V) within the 300–800 nm range. The inside plot displays this emission spectrum zoomed on the UV part of the light

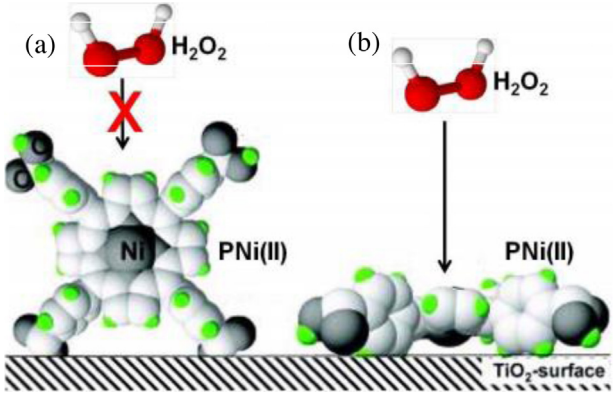

Fig. 6. TCPPNi geometry and interaction with TiO_2 surface and H_2O_2.

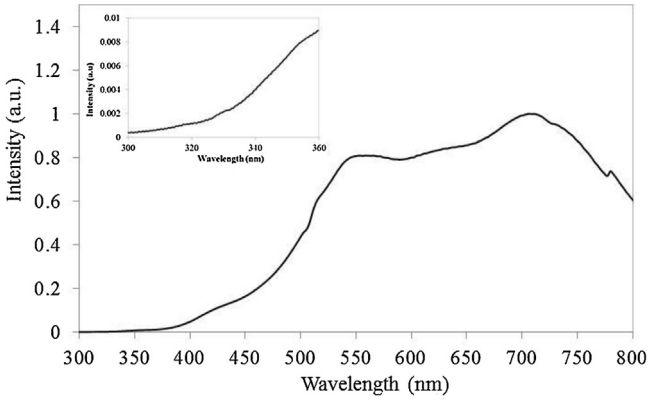

Fig. 7. Normalized emission spectrum of the polychromatic light source (halogen lamp powered at 110 V) between 300 and 800 nm.

region (300–360 nm). Experiments were performed at different intensities of halogen lamp power supply (HLps), from 110 to 220 V. The resulting changes in the lamp emission spectrum in the UV-part region (300–360 nm) are compared in Fig. 8(a) ($\lambda \approx 360$ nm corresponds to UV-light absorption limit of H_2O_2). From these emission spectra, the apparent intensity (I_{app}, counts) of UV part of the light source on a wavelength range can be calculated by numeric integration.

Fig. 8(b) shows the behaviour of $I_{0(app)}$ in the 300–360 nm range (counts) in relation to the lamp power supply (HLps,V). $I_{0(app)}$ increased exponentially (0, 0.5×10^4, 3.5×10^4, 11×10^4 and 29×10^4 counts) together with the increase in HLps = 0, 110, 150, 180 and 220 V, respectively. Fig. 9(a) compares the evolution of the H_2O_2 concentration in relation to time at different $I_{0(app)}$ values. In all cases, the concentration of H_2O_2 decreased linearly with the reaction time, indicating that H_2O_2-photolysis follows a zero-kinetics order ($r_{0H_2O_2} = k_0$, Eq. (8)), as previously observed by Li et al. [10]. k_0 represents the zero-order constant at a $I_{0(app)}$ value. In addition, the initial H_2O_2 photodecomposition rate ($r_{0H_2O_2}$) increased from 0.5×10^{-6} to 5×10^{-6} mol L^{-1} s^{-1} together with the increase in $I_{0(app)}$. We can therefore conclude that k_0 depends on the apparent light intensity value ($k_0 = k_I\ I_{0(app)}$ if a linear dependency is assumed).

$$-\frac{dC_0}{dt} = k_0 \tag{8}$$

$$r_{H_2O_2} = k_I I_{0(app)} \approx -\Phi_T I_0 \tag{9}$$

in the case of linear dependency.

Finally, Fig. 9(b) shows the changes in the $r_{0H_2O_2}$ with the apparent intensity (counts) in the 300–360 nm range. This indicates that the general H_2O_2-photolysis rate ($r_{H_2O_2}$) is a linear function of the incident UV part of the light intensity expressed by Eq. (9). This expression corresponds to the second method proposed by Crittenden, et al. [31], where k_I can be related to the overall quantum yield of H_2O_2-photolysis under UV part of the light.

Following these results, the photocatalytic degradation of H_2O_2 with non-doped and TCPPNi-doped TiO_2 was performed at the lowest lamp power supply (110 V, in the 300–800 nm range, Fig. 7), in order to limit the effect of UV part of the light irradiation on the H_2O_2 degradation (in the 300–380 nm range), which corresponded to 0.4% of the total light intensity emission of the halogen lamp. The H_2O_2 decomposition with non-doped and TCPPNi-doped TiO_2 was measured for 90 min in the dark followed by 60 min under light (Fig. 10). In the dark, no H_2O_2 degradation was observed for P25, Ni/5 and Ni/6, while a small decrease was observed for the other TCPPNi-doped catalysts. Under light, the H_2O_2 was found to be degraded by P25 and TCPPNi-doped TiO_2. However, the degradation rate was higher under light than in the dark for all the catalysts and depended on the TCPPNi concentration with the highest H_2O_2 degradation with catalyst PNi/3.

4. Discussion

The nitrogen adsorption/desorption isotherms observed in the present study are characteristic of non-porous materials. The S_{BET} was found to be the same for all the catalysts (50 ± 5 m^2 g^{-1}), corresponding to the theoretical value of the Degussa P25 TiO_2. So the chimisorption of TCPPNi onto Degussa P25 TiO_2 did not modify the specific surface area, S_{BET}.

The main absorption edge, shown in the DR-UV/vis spectra (Fig. 1), corresponds to the absorption of TiO_2-anatase [29]. No shift of this band was observed in the present study when TCPPNi was chimisorbed onto the Degussa P25 TiO_2. Thus, it can be concluded that TCPPNi did not modify the band-gap of TiO_2. Indeed, the goal of doping TiO_2 with porphyrins, which are sensitive to visible light, is to make TiO_2 sensitive to visible light through the following mechanism: when a doped sample is illuminated with visible light, an electron is promoted from the HOMO band (Highest Occupied Molecular Orbital) of the porphyrin to its LUMO band (Lowest Unoccupied Molecular Orbital) and that excited electron is subsequently transferred to the conduction band of TiO_2. The Soret and the Q bands, which are characteristic porphyrin peaks, are observable in visible wavelengths. In the present study, the position of the maximum of the Soret band of TCPPNi varied between the catalysts and was found to depend on the concentration of TCPPNi (Fig. 2). Indeed, the Soret band was observed at 415 nm for PNi/1, 407 nm for PNi/2 and between 402 and 404 nm for catalysts PNi/3 to PNi/6. This shift depends on the electrostatic force of attraction and can be interpreted in terms of an increase in the delocalization of the π orbital of the porphyrin in the TiO_2 conduction band. In the literature, a large shift has been attributed firstly, to a strong interaction between the TCPPNi and the TiO_2 surface and secondly, to the delocalized π^* state of the porphyrin derivative in the TiO_2 conduction band, in the same manner as the Ru complex [32,33]. This strong interaction is accomplished through a chemical linkage between the dye molecules and the surface of the semiconductors. Ma et al. [34] report that the difference in the interaction is considered to result from the difference in the adsorption mode of the dye on the TiO_2 surface. They also report that the number of carboxyl groups has an important effect on the adsorption behaviour. An interaction between a porphyrin and the TiO_2 surface with only one carboxyl group is weaker than with four carboxyl groups, and the band shift observed for the first case is smaller than for the second. In Fig. 2, the absorbance peak maximum of the Soret band is reported in relation to TCPPNi concentration chimisorbed onto TiO_2. For low concentrations, *i.e.*, PNi/1 and PNi/2, the shift is large

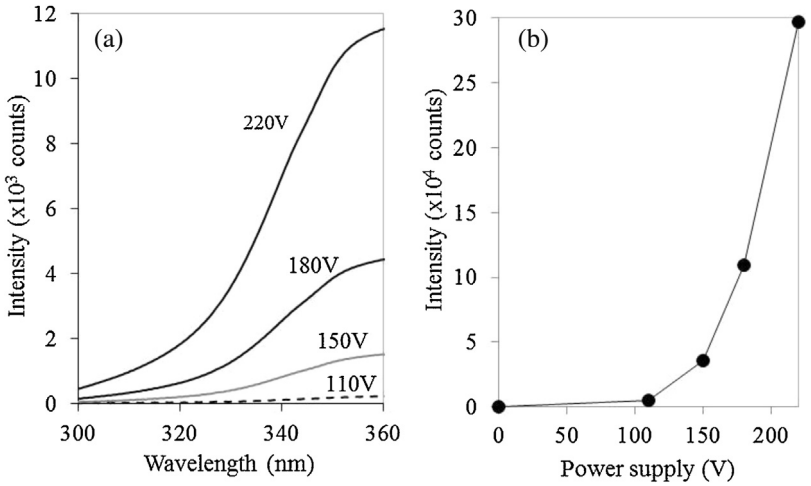

Fig. 8. (a) Emission spectrum between 300 and 360 nm of the halogen lamp at different power supplies. (b) Intensity of the halogen lamp in relation to power supply.

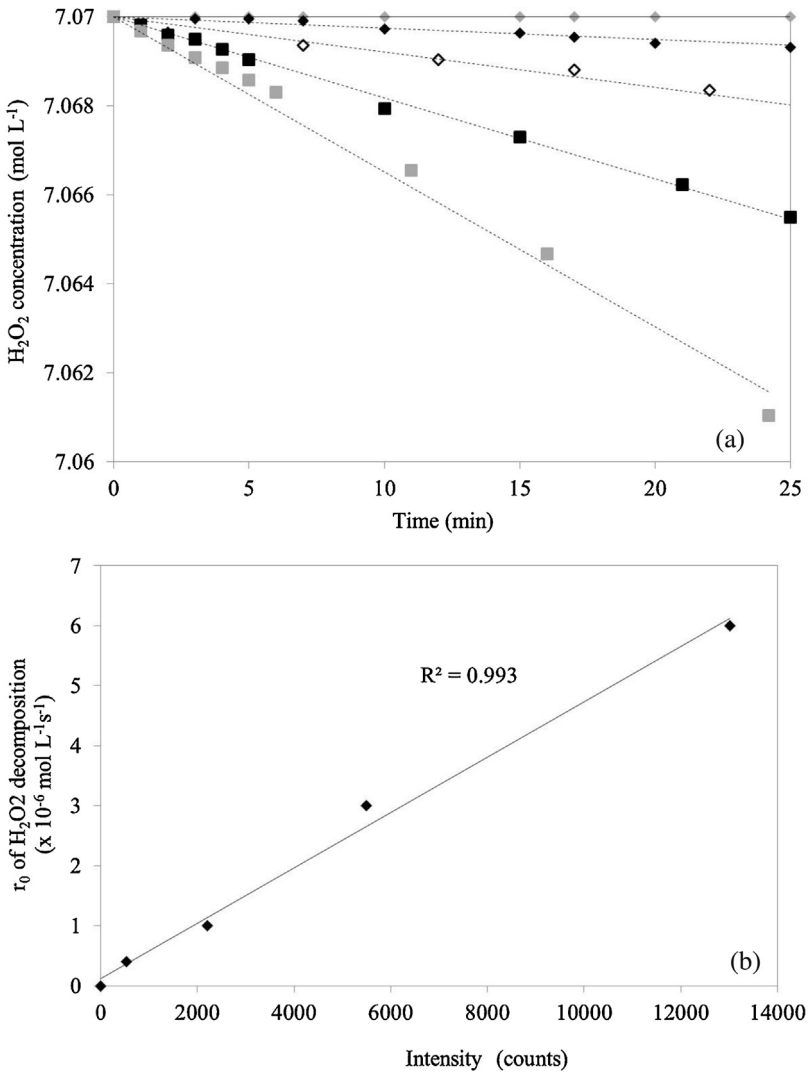

Fig. 9. (a) H_2O_2 degradation over time with different intensities of light power supply: 0 (♦), 110 (♦), 150 (◇), 180 (■) and 250 V (■). (b) Rate of H_2O_2 decomposition at different intensities.

(±10 nm), so the interaction is strong, probably involving with the four carboxyl groups as illustrated in Fig. 6(b). By contrast, for high concentrations, *i.e.*, PNi/3 to PNi/6, the shift is small (±3 nm), so the interaction is weak, probably involving with one or two carboxyl groups as illustrated in Fig. 6(a). The concentration of TCPPNi may explain the different interaction modes with TiO_2. Campbell et al.

[35] report that the presence of four carboxylic groups might force the TCPPNi to lie flat on the TiO_2 surface, as observed at low TCPPNi concentrations. However, at high TCPPNi concentrations, the steric hindrance of the TCPPNi prevents TCPPNi linkage through the four carboxylic groups [36], which explains the weaker interaction in the presence of one or two carboxyl groups.

These observations were confirmed by FT-IR measurements, which showed the characteristic vibrations of the TiO_2 structure. The stretch observed at 3300 and 1630 cm^{-1} corresponds to —OH groups and H_2O molecules being adsorbed on the TiO_2 surface [37]. However, between 1200 and 1800 cm^{-1}, vibrations observed for TCPPNi-doped catalysts were quite different than for P25 (Fig. 3). As the characteristic vibrations of tetra(4-carboxyphenyl) porphyrin are reported in this region [38–40], the differences observed could be due to the TCPPNi chimisorption. In the TCPPNi-doped catalysts, vibrations at 1630 cm^{-1} were observed in all the catalysts, but they were more intense for the TCPPNi-doped catalysts than for Degussa P25 TiO_2. Moreover, vibrations were observed at 1400 cm^{-1} in the TCPPNi-doped catalysts only and the intensity was found to increase with the TCPPNi concentration. Finally, some vibrations corresponding to the vibrations of TCPPNi appeared at 1350 cm^{-1} for PNi/5 and PNi/6 (Fig. 3(b)). These data confirm that TCPPNi was present at the surface on Degussa P25 TiO_2. Moreover, the increase in TCPPNi concentration was related to the increase in peak intensity and to the appearance of the peak at 1350 cm^{-1}. According to the literature, the disappearance of the vibration at 1700 cm^{-1} (C═O) and the presence of vibration observed at 1630 and 1400 cm^{-1}, usually attributed to COO^- asymmetric and symmetric stretches, indicate a chemisorption of the TCPPNi on TiO_2 surface through the carboxyl group [34,36,41,42]. The same trend was observed in the TCPPNi-doped catalysts with the disappearance of the vibration observed at 1700 cm^{-1} (C═O) and its presence observed at 1630 and 1400 cm^{-1} (Fig. 3). Thus, the stretches observed between 1200 and 1800 cm^{-1} establish that a chemical interaction took place between TCPPNi and Degussa P25 TiO_2 *via* the carboxylic group. These data confirm the observations made by the DR-UV/vis measurements. We can therefore conclude that the linkage through carboxyl groups serves to enhance the transfer of electrons between the π^* orbitals of the porphyrin and the Ti(3d) orbital of TiO_2. This coupling leads to increased delocalization of the π^* level of the porphyrin. The energy of the π^* level of the porphyrin is decreased by this delocalization, which explains the observed shift of the Soret peaks [33].

TG analyses confirmed these observations (Fig. 4). The temperature at which TCPPNi degradation took place is equal to 350 °C. The loss of weight and the exothermic peaks associated in Fig. 4 for all the catalysts correspond to the degradation of TCPPNi. Two distinct groups were observed. At high TCPPNi concentrations, *i.e.*, catalysts PNi/4, PNi/5 and PNi/6, the exothermic peak was observed at around 355 °C, while at low TCPPNi concentrations, *i.e.*, catalysts PNi/1, PNi/2 and PNi/3, the exothermic peak was observed at around 420 °C. A degradation at a temperature higher than the free TCPPNi could mean that the TCPPNi was linked more strongly to the TiO_2 surface at low TCPPNi concentrations (PNi/1) than at high TCPPNi concentrations (PNi/6). The DR-UV/vis and FTIR measurements highlight the fact that the TCPPNi was linked through 4 carboxyl groups at low TCPPNi concentrations (PNi/1, PNi/2 and PNi/3) and through only 1 or 2 carboxyl groups at high TCPPNi concentrations (PNi/4, PNi/5 and PNi/6).

The fluorescence microscopy pictures of catalysts PNi/3 and PNi/5 confirm that the TCPPNi was located around Degussa P25 TiO_2 (Fig. 5). Indeed, the TCPPNi was found to emit wavelengths equal to 675 and 725 nm, which correspond to red wavelengths [43]. Particles of Degussa P25 TiO_2 without porphyrin were blue (Fig. 5a). With the presence of only a few porphyrins, the Degussa P25 TiO_2 was still excited by light emitted by the microscope, as shown by the fact that particles of catalyst PNi/3 were purple (blue + red) (Fig. 5b). So, we can conclude that the TCPPNi did not cover the entire surface of the Degussa P25 TiO_2. Finally, at high TCPPNi concentrations, the Degussa P25 TiO_2 was no longer excited by light emitted by the microscope, as shown by the fact that particles of catalyst PNi/5 were red. So, we can conclude that, in this case, the TCPPNi did cover the entire surface of the Degussa P25 TiO_2.

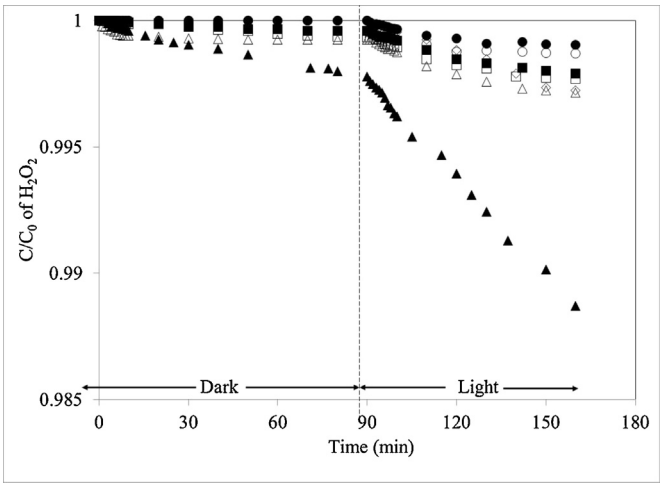

Fig. 10. Degradation of H_2O_2 after 90 min in the dark followed by 60 min under light with catalysts P25 (◊), PNi/1 (■), PNi/2 (□), PNi/3 (▲), PNi/4 (Δ), PNi/5 (●) and PNi/6 (○).

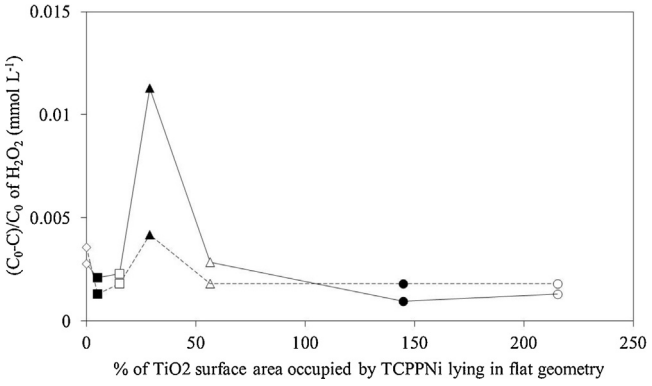

Fig. 11. Maximum degradation of H_2O_2 after 90 min in the dark (---) followed by 60 min under light (—) with catalysts P25 (◊), PNi/1 (■), PNi/2 (□), PNi/3 (▲), PNi/4 (Δ), PNi/5 (●) and PNi/6 (○) in relation to the percentage of TiO_2 surface area occupied by TCPPNi lying in flat geometry.

The linear decrease in H_2O_2 concentration without a catalyst at different lamp intensities corresponds to a zero-order kinetic, as previously reported by Jenny et al. [14] and Li et al. [10] for the photodecomposition of H_2O_2 on a TiO_2 surface under visible light.

Our results show that the degradation of H_2O_2 in the dark and under light varied with the TCPPNi concentration (Fig. 10), with an optimal activity being found with PNi/3 (Fig. 11). As described above, the TCPPNi concentration reflects the percentage of TiO_2 surface area covered by porphyrin and the linkage mode of TCPPNi on TiO_2, which influences the interaction between the two.

The H_2O_2 degradation observed in the dark could be a result of Fenton-like reactions due to the Ni(II) center of the TCPPNi. This kind of reaction occurs when H_2O_2 has access to and reacts directly with the Ni(II). This is possible only when the TCPPNi is lying in a flat geometry, anchored to the TiO_2 through four carboxylic groups (Fig. 6b), as is the case at low TCPPNi concentrations. At higher TCPPNi concentrations, the level of H_2O_2 degradation in the dark is

nil. In this case, the TCPPNi is in an edgewise geometry, the Ni(II) centre is less accessible for H_2O_2 (Fig. 6a) and the Fenton-like reactions do not occur.

Under light, the H_2O_2 degradation rate increases compared to the one in the dark with, again, the best activity being observed for PNi/3 (Fig. 10). The influence of porphyrin concentration on photocatalytic activity has been previously reported for the degradation of *p*-nitrophenol with porphyrin-doped TiO_2 [44]. In the present case, the TCPPNi concentration was found also to influence the degradation of H_2O_2. At low concentrations, the TCPPNi was observed to be anchored to the TiO_2 through the four carboxylic groups, which might improve the transfer of electrons between excited TCPPNi and the TiO_2 conduction band, as observed by Campbell et al. [35] and Chen et al. [41]. The nickel center of the TCPPNi was also made more accessible for the degradation of H_2O_2 through Fenton-like reactions (Fig. 6). At high TCPPNi concentrations, the level of photoactivity was found to decrease (PNi/4, PNi/5 and PNi/6) (Fig. 11). The TCPPNi was anchored through only one or two carboxylic groups. The rate of electron transfer may have been lower and the nickel centre of the TCPPNi became less accessible for the degradation of H_2O_2 through Fenton-like reactions (Fig. 6a). Moreover, in the flat geometry configuration, the TCPPNi was found to cover more than 50% of the TiO_2 surface area of the catalysts PNi/4, PNi/5 and PNi/6. It seems that more than 50% of the TiO_2 surface area needs to be available in order for TiO_2 to be activated by UV part of the light and for H_2O_2 degradation to take place. Yet, to improve substantially the photoactivity of TiO_2 with TCPPNi, it is necessary to photoexcite both the components of the system, *i.e.*, TiO_2 and the sensitizer. The beneficial effect on the photoactivity is due to a cooperative mechanism [45,46]. The H_2O_2 degradation observed was due to (i) the photoactivity of TiO_2, (ii) a Fenton-like reaction, (iii) the photoactivity of TCPPNi and (iv) the interaction between TCPPNi and TiO_2.

5. Conclusions

The nickel tetra(4-carboxyphenyl) porphyrin (TCPPNi) was chimisorbed onto the Degussa P25 TiO_2 at different concentrations (0.002, 0.006, 0.0115, 0.0225, 0.0575 and 0.0855 mol TCPPNi × g^{-1} P25). The anchoring mode of the TCPPNi was determined by diffuse reflectance in the UV/vis region, Fourier transform infrared combined with thermal gravimetry and differential scanning calorimetry measurements. This anchoring to the Degussa P25 TiO_2 took place through the four carboxylic groups at low TCPPNi concentrations. In this case, the TCPPNi was lying in a flat geometry. At higher concentrations, characteristics of free TCPPNi were observed, meaning that the anchoring was occurring through one or two carboxylic groups. In that case the TCPPNi was in an edgewise geometry. The level of H_2O_2 degradation was used to evaluate the activity of the catalysts. This activity was related to the TCPPNi anchoring mode. At low concentrations, the TCPPNi was anchored through the four carboxylic groups. In this case, the nickel centre was accessible to the H_2O_2 molecule and the Degussa P25 TiO_2 could be activated by light. By contrast, at high TCPPNi concentrations, in the edgewise geometry of TCPPNi, H_2O_2 access to the nickel centre was not easy and the Degussa P25 TiO_2 was not activated by light. This meant that the level of H_2O_2 degradation decreased and an optimum H_2O_2 degradation was observed.

Acknowledgements

L.T. is grateful to the Belgian Fonds pour la Formation à la Recherche dans l'Industrie et dans l'Agriculture, F.R.I.A., and the University of Liege for their award of a PhD grant. C.A.P. and S.D.L. are grateful to F.R.S.-FNRS for their respective post-doctoral research and research associate positions. The authors would like to thank Pr. Jean-Paul Pirard and Pr. Bernard Gilbert (University of Liege), and Pr. Dirk Poelman (University of Ghent) for their helpful discussions. The authors also acknowledge the Fonds de la Recherche Fondamentale Collective (F.R.F.C), the Interuniversity Attraction Pole (IAP-P6/17) and the Ministère de la Région Wallonne for their financial support.

References

[1] A. Fujishima, K. Honda, Nature 238 (1972) 37–38.
[2] S. Malato, Emerging Contaminants from Industrial and Municipal Waste: Removal Technologies, Springer, Berlin/Heidelberg, 2008, pp. 177–197.
[3] P. Gogate, A.B. Pandit, Adv. Environ. Res. 8 (2004) 501–551.
[4] D. Chen, A.K. Ray, Water Res. 32 (1998) 3223–3234.
[5] C. Kormann, D.W. Bahnemann, M.R. Hoffmann, J. Phys. Chem. 92 (1988) 5196–5201.
[6] I.K. Konstantinou, T.A. Albanis, Appl. Catal. B: Environ. 49 (2004) 1–14.
[7] D.S. Bhatkhande, V.G. Pangarkar, A.A.C.M. Beenackers, J. Chem. Technol. Biotechnol. 77 (2002) 102–116.
[8] A. Fujishima, X. Zhang, D.A. Tryk, Surf. Sci. Rep. 63 (2008) 515–582.
[9] T. Hirakawa, K. Yawata, Y. Nosaka, Appl. Catal. A: Gen. 325 (2007) 105–111.
[10] X. Li, C. Chen, J. Zhao, Langmuir 17 (2001) 4118–4122.
[11] T. Hirakawa, Y. Nosaka, Langmuir 18 (2002) 3247–3254.
[12] H. Bader, V. Sturzenegger, J. Hoigne, Water Res. 22 (1988) 1109–1115.
[13] H. Goto, Y. Hanada, T. Ohno, M. Matsumura, J. Catal. 225 (2004) 223–229.
[14] B. Jenny, P. Pichat, Langmuir 7 (1991) 947–954.
[15] C.A. Páez, D.Y. Liquet, C. Calberg, S.D. Lambert, I. Willems, A. Germeau, J.-P. Pirard, B. Heinrichs, Catal. Commun. 15 (2011) 132–136.
[16] S.B. Kanungo, K.M. Parida, B.R. Sant, Electrochim. Acta 26 (1981) 1157–1167.
[17] B. Ahmed, H. Mohamed, E. Limem, B. Nasr, Ind. Eng. Chem. Res. 48 (2009) 3370–3379.
[18] S.B. Kanungo, J. Catal. 58 (1979) 419–435.
[19] S.-S. Lin, M.D. Gurol, Environ. Sci. Technol. 32 (1998) 1417–1423.
[20] C.B. Roy, J. Catal. 12 (1968) 129–133.
[21] M. Auriere, G.A. Wade, F. Lignieres, A. Hui-Bon-Hoa, J.D. Landstreet, I.K. Iliev, J.F. Donati, P. Petit, T. Roudier, S. Theado, Astron. Astrophys. 523 (2010).
[22] N. Kitajima, S. Fukuzumi, Y. Ono, J. Phys. Chem. 82 (1978) 1505–1509.
[23] J.R. Goldstein, A.C.C. Tseung, J. Catal. 32 (1974) 452–465.
[24] M.A. Hasan, M.I. Zaki, L. Pasupulety, K. Kumari, Appl. Catal. A: Gen. 181 (1999) 171–179.
[25] M. Casas-Cabanas, G. Binotto, D. Larcher, A. Lecup, V. Giordani, J.M. Tarascon, Chem. Mater. 21 (2009) 1939–1947.
[26] C.A. Páez, S.D. Lambert, D. Poelman, J.-P. Pirard, B. Heinrichs, Appl. Catal. B: Environ. 106 (2011) 220–227.
[27] L. Tasseroul, S.L. Pirard, S.D. Lambert, C.A. Páez, D. Poelman, J.-P. Pirard, B. Heinrichs, Chem. Eng. J. 191 (2012) 441–450.
[28] A.D. Adler, F.R. Longo, J.D. Finarelli, J. Goldmacher, J. Assour, L. Korsakoff, J. Org. Chem. 32 (1967) 476.
[29] B. Braconnier, C.A. Páez, S. Lambert, C. Alié, C. Henrist, D. Poelman, J.-P. Pirard, R. Cloots, B. Heinrichs, Microporous Mesoporous Mater. 122 (2009) 247–254.
[30] A.J. Lecloux, Catalysis: Science and Technology, in: J.R. Anderson, M. Boudart (Eds.), Springer, Berlin, 1981, pp. 171–230.
[31] J.C. Crittenden, S. Hu, D.W. Hand, S.A. Green, Water Res. 33 (1999) 2315–2328.
[32] M.K. Nazeeruddin, A. Kay, I. Rodicio, R. Humphry-Baker, E. Mueller, P. Liska, N. Vlachopoulos, M. Graetzel, J. Am. Chem. Soc. 115 (1993) 6382–6390.
[33] T. Ma, K. Inoue, H. Noma, K. Yao, E. Abe, J. Photochem. Photobiol. A 152 (2002) 207–212.
[34] T. Ma, K. Inoue, K. Yao, H. Noma, T. Shuji, E. Abe, J. Yu, X. Wang, B. Zhang, J. Electroanal. Chem. 537 (2002) 31–38.
[35] W.M. Campbell, A.K. Burrell, D.L. Officer, K.W. Jolley, Coord. Chem. Rev. 248 (2004) 1363–1379.
[36] K.S. Finnie, J.R. Bartlett, L. Woolfrey, Langmuir 14 (1998) 2744–2749.
[37] T. Bezrodna, G. Puchkovska, V. Shymanovska, J. Baran, H. Ratajczak, J. Mol. Struct. 700 (2004) 175–181.
[38] G. Granados-Oliveros, E.A. Páez-Mozo, F.M. Ortega, C. Ferronato, J.-M. Chovelon, Appl. Catal. B: Environ. 89 (2009) 448–454.
[39] M.A. Schiavon, L.S. Iwamoto, A.G. Ferreira, Y. Iamamoto, M.V.B. Zanonic, M.D.D. Assisa, J. Braz. Chem. Soc. 11 (2000) 458–466.
[40] N. Datta-Gupta, T.J. Bardos, J. Heterocycl. Chem. 3 (1966) 495–502.
[41] D. Chen, D. Yang, J. Geng, J. Zhu, Z. Jiang, Appl. Surf. Sci. 255 (2008) 2879–2884.
[42] C.E. Diaz-Uribe, M.C. Daza, F. Martínez, E.A. Páez-Mozo, C.L.B. Guedes, E. Di Mauro, J. Photochem. Photobiol. A 215 (2010) 172–178.
[43] F. Odobel, E. Blart, M. Lagrée, M. Villieras, H. Boujtita, N. El Murr, S. Caramori, C. Alberto Bignozzi, J. Mater. Chem. 13 (2003) 502–510.
[44] L. Tasseroul, S.D. Lambert, D. Eskenazi, M. Amoura, C.A. Páez, S. Hiligsmann, P. Thonart, B. Heinrichs, J. Photochem. Photobiol. A 272 (2013) 90–99.
[45] C. Wang, J. Li, G. Mele, G.-M. Yang, F.-X. Zhang, L. Palmisano, G. Vasapollo, Appl. Catal. B: Environ. 76 (2007) 218–226.
[46] G. Mele, R.D. Sole, G. Vasapollo, G. Marcı, E. Garcìa-Lòpez, L. Palmisano, J.M. Coronado, M.D. Hernández-Alonso, C. Malitesta, M.R. Guascito, J. Phys. Chem. B 109 (2005) 12347–12352.